LHB

Hydroscience Journal

ISSN: (Print) (Online) Journal homepage: https://www.tandfonline.com/loi/tlhb21

Computation fluid dynamics investigation of the flow in junctions: application to hydraulic short circuit operating mode

Jean Decaix, Mathieu Mettille, Jean-Louis Drommi, Nicolas Hugo & Cécile Münch-Alligné

To cite this article: Jean Decaix, Mathieu Mettille, Jean-Louis Drommi, Nicolas Hugo & Cécile Münch-Alligné (2023) Computation fluid dynamics investigation of the flow in junctions: application to hydraulic short circuit operating mode, LHB, 109:1, 2290025, DOI: 10.1080/27678490.2023.2290025

To link to this article: https://doi.org/10.1080/27678490.2023.2290025

© 2024 The Author(s). Published by Informa UK Limited, trading as Taylor & Francis Group.

Published online: 19 Jan 2024.

Submit your article to this journal

View related articles

Full Terms & Conditions of access and use can be found at
https://www.tandfonline.com/action/journalInformation?journalCode=tlhb21

LHB: HYDROSCIENCE JOURNAL
2023, VOL. 109, 2290025
https://doi.org/10.1080/27678490.2023.2290025

OPEN ACCESS Check for updates

Computation fluid dynamics investigation of the flow in junctions: application to hydraulic short circuit operating mode

Jean Decaix[a], Mathieu Mettille[a], Jean-Louis Drommi[b], Nicolas Hugo[c] and Cécile Münch-Alligné[a]

[a]Institute of Sustainable Energy, School of Engineering, Sion, Switzerland; [b]EDF CIH DT, Chambéry, France; [c]Alpiq, Lausanne, Switzerland

ABSTRACT

Due to the penetration of stochastic low-carbon sources of production, requirements for flexible generation increase. The flexibility of pumped storage hydropower plants in pump mode can be improved by implementing hydraulic short circuit modes, which consists in operating the turbine(s) and the pump(s) in parallel. This new operating mode can be investigated by computational fluid dynamics to determine the head losses and to investigate the flow topology. Nine geometries of the Grand'Maison and Forces Motrices Hongrin-Léman (FMHL/FMHL+) plants are considered. Due to the lack of measurements, simulations are performed using different turbulence models and meshes to assess the uncertainty of the results. A statistical analysis of the results shows that low values of the head loss coefficients are obtained for geometries that limit the impingement of the flow on the walls and the development of a swirling flow downstream. Such geometries have the benefit of also limiting the wall pressure fluctuations and wall shear stresses, i.e. the risk of cavitation and the abrasion of the pipe walls due to sediment transport. These new results for the hydropower community are valuable for owners in implementing hydraulic short circuit mode in existing power plants or in designing new suitable junctions.

KEYWORDS

CFD; RANS; hydraulic short-circuit; Ansys® Fluent®; A\nsys® CFX®; OpenFOAM

1. Introduction

The electric power sector has been undergoing a great change for the last two decades due to the penetration of new renewable energies such as solar panels and wind turbines but also due to a higher demand in flexibility (Martinot, 2016). Hydropower is a low-carbon renewable energy that was used for decades as a flexible method for power generation and storage of electricity (Guittet et al., 2016). However, the flexibility of hydropower can still be enhanced, mainly for pumped storage power plants (Pérez-Díaz, Cavazzini et al., 2014), for instance by implementing the hydraulic short circuit (HSC) operating mode (Pérez-Díaz, Sarasúa et al., 2014), which consists in operating pump(s) and turbine(s) in parallel. Usually, the pumps operate at a fixed operating point, i.e. their energy consumption is fixed. While most turbines, such as Pelton or Francis turbines, are regulated in power, thanks to needles or guides vanes, in HSC operating mode, the discharge through the turbine(s) can be adjusted in such a way that the energy consumed by the power plant regarding to the grid is no longer fixed, which provides new flexibility to the electrical network. The HSC operating mode has already been implemented in some power plants such as Forces Motrices Hongrin-Léman (FMHL+) in Switzerland (Micoulet et al., 2016) or Kops II in Austria (Meusburger, 2009) and is in progress at the Grand'Maison power plant (*France's Grand Maison plant testing HSC technology*, 2022) in the framework of the XFLEX-HYDRO H2020 project.

The implementation of HSC mode requires upstream studies to verify the possibility of operating this mode without risks. Among them, one-dimensional transient analyses are of the greatest importance (Landry et al., 2022; Nicolet et al., 2019). Investigating the flows in the junctions by means of experiments or computational fluid dynamics (CFD) to determine the head losses, to study the flow topology and the structural load, is also necessary (Decaix et al., 2021; Decaix, Drommi et al., 2022; Huber et al., 2005; Khalfaoui et al., 2022; Morabito et al., 2022). Since the topic is rather new for the hydraulic community, the relevant literature is still sparse. A recent paper discussing the hydrodynamic processes in angular fitting connections shows that the use of an equivalent length is not accurate enough compared to CFD results, which suggest that CFD calculations are necessary to assess head losses in complex pipe systems (Karpenko et al., 2023).

The present paper aims at describing the methodology used for the CFD calculations, mainly to validate and quantify the uncertainties regarding the predictions of the head loss coefficients, the flow topology,

CONTACT Jean Decaix jean.decaix@hevs.ch

© 2024 The Author(s). Published by Informa UK Limited, trading as Taylor & Francis Group.
This is an Open Access article distributed under the terms of the Creative Commons Attribution-NonCommercial License (http://creativecommons.org/licenses/by-nc/4.0/), which permits unrestricted non-commercial use, distribution, and reproduction in any medium, provided the original work is properly cited. The terms on which this article has been published allow the posting of the Accepted Manuscript in a repository by the author(s) or with their consent.

the wall pressure and the wall shear stress. Overall, nine geometries are considered, including T-junctions for which analytical formulas are available and two and three junctions from the Grand'Maison and FMHL/FMHL+ power plants, respectively. For each geometry, several discharge ratios are computed using different meshes, turbulence models and solvers.

The paper is structured as follows: firstly, the methodology is described; secondly, a validation of the simulation set-up is carried out by considering three T-junctions and a Y-junction to quantify the uncertainty between different numerical set-ups and analytical formulae (only for the T-junctions); then, the results obtained for five "real" bifurcations are discussed and compared in detail; finally, the paper ends with a general conclusion.

2. Methodology

2.1. Simulation strategy

Because there are few references available in the literature regarding the fluid simulations of the HSC mode, and since no measurements are available for the test cases of the Grand'Maison and FMH/FMHL+ power plants, a simulation strategy has been designed. This strategy consists in performing several steady-state simulation of the same geometry and operating point using different turbulence models, meshes and software. Then a statistical analysis of the results is performed by computing the average and the standard deviation (eventually the minimum and maximum) of the head loss coefficients. If the standard deviation is small, it means that all the simulations predict the same flow. Therefore, the results can be considered with a certain level of confidence. Otherwise, the uncertainty is higher, which may be due to the development of flow unsteadiness. In that case, unsteady-state simulations of the operating can be performed to check whether the result discrepancy decreases. This operating point can also be selected for a detailed on-site investigation.

2.2. Numerical set-up

The flow is modelled by the incompressible Reynolds-averaged Navier-Stokes equations, for which the Reynolds stresses are computed either using Boussinesq's assumption, which requires the computation of an eddy viscosity (Durbin, 2011), or an explicit algebraic relation (Wallin & Johansson, 2000). The eddy viscosity is computed by solving two additional transport equations that depend on the turbulence model chosen. For this study, three turbulence models are considered: the Renormalisation Group (RNG) k-ε (Yakhot et al., 1992), the realisable k-ε (Shih et al., 1994) and the SST (Menter, 2009) models. Simulations have been performed using different meshes that differ in element shape (hexahedrons, tetrahedrons, polygons ...). However, all meshes are generated following standard guidelines (Menter et al., 2021), mainly regarding the addition of prism layers close to the wall to accurately capture the boundary layer, as discussed later in the text. The y^+ values range from 80 to 300, which agrees with the use of a wall function to model the boundary layer. The flow is simulated with one of three software programs: Ansys® Fluent®, Ansys® CFX® and OpenFOAM. Regardless of the software used, the convective fluxes are discretised with a high-order scheme. The set of equations is solved either with the segregated Semi-Implicit Method for Pressure-Linked Equations (SIMPLE) algorithm for the OpenFOAM and Ansys® Fluent® simulations or a coupled algorithm for the Ansys® CFX® simulations.

2.3. Definition of the partial head loss coefficient

The loss coefficients K_{ij} in a bifurcation are defined by Equation (1).

$$K_{ij} = \frac{\Delta\overline{p_{tot}}}{\frac{1}{2}\rho C_1^2} \tag{1}$$

Where i and j are indices referring to the pipes considered (see Figure 1(a)); $\Delta\overline{p_{tot}}$ is the difference of the surface average total pressure between two cross sections located in pipe i and pipe j, respectively; ρ is the fluid density; and C_1 is the discharge velocity in pipe 1. In cases where the sections i and j are far from the bifurcation, the linear head losses are subtracted to obtain only the loss coefficient associated with the bifurcation.

Equation (1) is derived using the demonstration hereafter based on the book of Comolet (2006). The overall power losses ΔP in the junction are defined by Equation (2).

$$\Delta P = P_1 - (P_2 + P_3) \tag{2}$$

where P_i denotes the power of fluid in section i defined by:

$$P_i = \iint \left(p + \rho g z + \frac{1}{2}\rho c^2\right) \boldsymbol{c} \cdot \boldsymbol{n}\, \mathrm{d}S_i \tag{3}$$

Where p is the pressure; g is the acceleration of gravity; z is the altitude; c is the fluid velocity, $\boldsymbol{c}$ is the velocity vector; and $\boldsymbol{n}$ is the unit normal vector to section S_i.

Then, by defining:

$$p^* = p + \rho g z \tag{4}$$

$$\overline{p^*} = \frac{\iint p^* \boldsymbol{c} \cdot \boldsymbol{n}\, \mathrm{d}S}{\iint \boldsymbol{c} \cdot \boldsymbol{n}\, \mathrm{d}S} \tag{5}$$

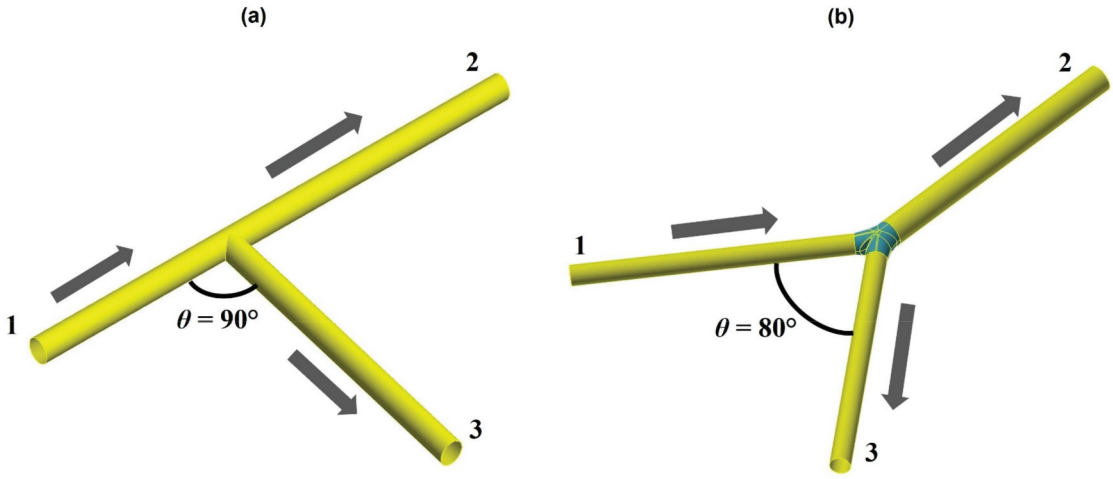

Figure 1. Geometries of the computational domain: (a) for the T-junction at 90 degrees, (b) for the Y-junction at 80 degrees. The arrows indicate the flow direction in each pipe.

$$\bar{c} = \frac{1}{S}\iint \boldsymbol{c}\cdot\boldsymbol{n}\,\mathrm{d}S = \frac{Q_v}{S} \tag{6}$$

$$\overline{c^2} = \left(\iint \frac{c^2}{\bar{c}^3 S}\boldsymbol{c}\cdot\boldsymbol{n}\,\mathrm{d}S\right)\bar{c}^2 = \alpha\bar{c}^2 \tag{7}$$

$$\overline{p_{tot}} = \overline{p^*} + \frac{1}{2}\rho\alpha\bar{c}^2 \tag{8}$$

where Q_v is the volumetric flow rate and $\boldsymbol{\alpha}$ is a coefficient close to 1 for a turbulent flow, Equation (2) can be rearranged as follows:

$$\Delta P = (\Delta\overline{p_{tot}})_{12}\ Q_{v,2} + (\Delta\overline{p_{tot}})_{13}\ Q_{v,3} \tag{9}$$

where $(\Delta\overline{p_{tot}})_{ij} = \overline{p_{tot}}_i - \overline{p_{tot}}_j$ can be interpreted as a partial loss if the difference is positive.

By introducing the coefficients K_{ij} defined by Equation (1) and the ratio $\gamma = Q_{v,2}/Q_{v,1}$, Equation (9) becomes:

$$\Delta P = \frac{1}{2}\rho c_1^2 Q_{v,1}(K_{12}\gamma + K_{13}(1-\gamma)) \tag{10}$$

where $(K_{12}\ \gamma)$ and $(K_{13}\ (1-\gamma))$ are partial head loss coefficients if they are positive. However, to compare different geometries, it is interesting to consider only the coefficients K_{ij}, since for a given discharge ratio γ, the higher K_{ij} is, higher are the losses. In the rest of the document, K_{ij} is referred to as a head loss coefficient.

3. Validation

3.1. T-junction

The first step in the validation of the numerical set-up and the methodology is performed by computing the flow in three T-junctions (Figure 1(a)), which differ by the angle θ between pipes 1 and 3. The diameter of each pipe is set to 3 m. The flow from pipe 1 is divided into pipe 2 and pipe 3. Pipe 1 extends over nine diameters upstream of the bifurcation, whereas pipes 2 and 3 extend 12 diameters downstream of the bifurcation. For these geometries and flow configurations, analytical formulae for the head loss coefficients derived from experiments are available in the literature (Gardel, 1957a, 1957b; Rennels, 2012; Ward-Smith, 1980).

The simulations are performed on two different meshes: a tetrahedral mesh generated using the Ansys ICEM CFD™ software with 1.3×10^6 cells and four prism layers attached to the wall (average $y^+ \approx 270$); a Cartesian mesh generated using the SnappyHexMesh tools with 1.5×10^6 cells and three prism layers attached to the wall (average $y^+ \approx 290$). Steady-state simulations of the flow are carried out with the SIMPLE algorithm and two software programs: Ansys® Fluent® 2019 R2 with the tetrahedral mesh and OpenFOAM 5 with the Cartesian mesh. For four sets of simulations, an arbitrary total pressure is set at the inlet of pipe 1 and the discharge is set at the outlet of pipes 2 and 3 to obtain the targeting discharge ratio. For the last set of simulations, a developed velocity profile is set at the inlet of pipe 1, an arbitrary pressure is set at the outlet of pipe 2 and the discharge is set at the outlet of pipe 3. The different configurations and set-ups are summarised in Table 1. Overall, 28 configurations have been simulated. For all the simulations, the Reynolds number in pipe 1 is around 6.8×10^6 for a pipe diameter of 3 m and a discharge of 16 $m^3\ s^{-1}$ and varies from 0.7×10^6 to 6.8×10^6 in pipes 2 and 3 according to the discharge ratio.

Figure 2(a) compares the head loss coefficients K_{12} and K_{13} predicted by the different simulations with three analytical formulae. For the head loss coefficient K_{13}, the simulations agree with the analytical formulae regardless of the inlet boundary condition in pipe 1. In contrast, for the head loss coefficient K_{12}, only the simulations for which a developed velocity profile is imposed at the inlet of pipe 1 match the analytical formulae for a discharge ratio lower than 0.5. At a larger discharge ratio, the simulations provide a better agreement with the data, even if for some set-ups an underestimation at discharge ratios higher

Table 1. Configurations and set-up of the 90 degree T-junction simulations.

Software	Mesh	Inlet boundary condition	Discharge ratio	Turbulence model
Ansys® Fluent®	Tetrahedral	Uniform velocity	0.0; 0.1; 0.25; 0.5; 0.75; 0.9; 1.0	SST realisable *k-ε*
OpenFOAM	Cartesian			RNG *k-ε*
		Developed velocity profile	0.0; 0.1; 0.27; 0.83	RNG *k-ε*

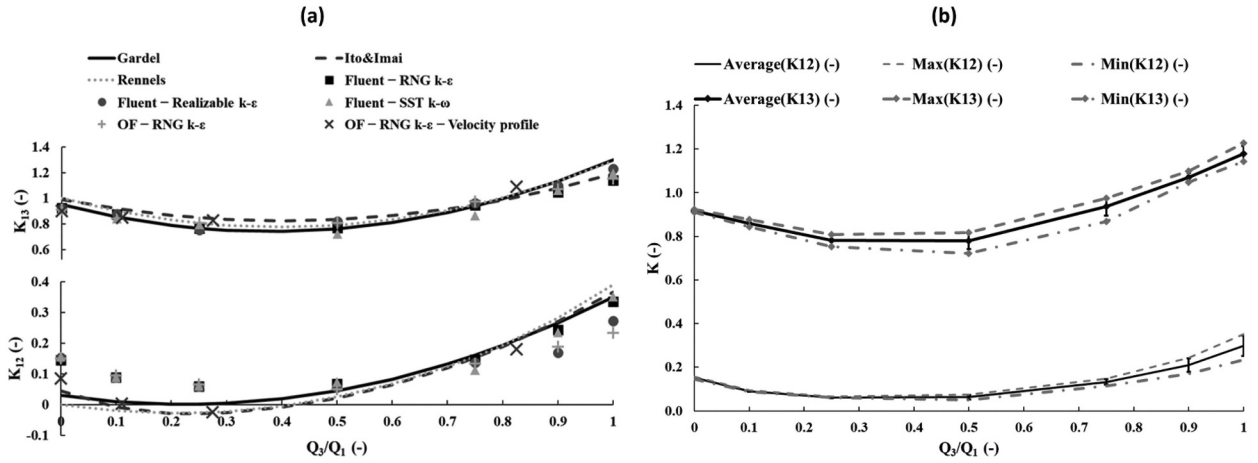

Figure 2. (a) Comparison of the head loss coefficients K_{12} and K_{13} predicted by CFD with various analytical formulae (the y-axis is deliberately clipped). (b) Statistical values of the head loss coefficients K_{12} and K_{13} predicted by CFD. The error bar denotes the standard deviation. T-junction at 90 degrees. OpenFoam (OF).

than 0.9 is observed, without a clear explanation. Figure 2(b) provides, for each discharge ratio, the average, standard deviation, maximum and minimum values of the head loss coefficients predicted by the 28 simulations. Overall, the discrepancy between the CFD results is around 15%, which is of the same order of magnitude as the differences between the analytical formulae. There is no clear influence on the CFD results of the turbulence model or of the mesh. For the head loss coefficient K_{12}, the dispersion of the results increases with the discharge ratio mainly for ratios of 0.9 and 1, perhaps due to the development of a large dead zone in pipe 2 that can influence the value of the total pressure.

Figure 3 compares the head loss coefficients for T-junctions at 100 and 80 degrees between the CFD results and the analytical formula available in the literature (Gardel, 1957a). The comparison follows the conclusion drawn for the T-junction at 90 degrees. The CFD results agree with the analytical formula, except for the values of the coefficient K_{12} for discharge ratios below 0.25 due to the imposed uniform velocity profile at the inlet section of pipe 1. The dispersion between the simulations increases with the increase in the discharge ratio. It seems that the Cartesian mesh often predicts a lower head loss coefficient for discharge ratio of 0.9 and 1, but this is

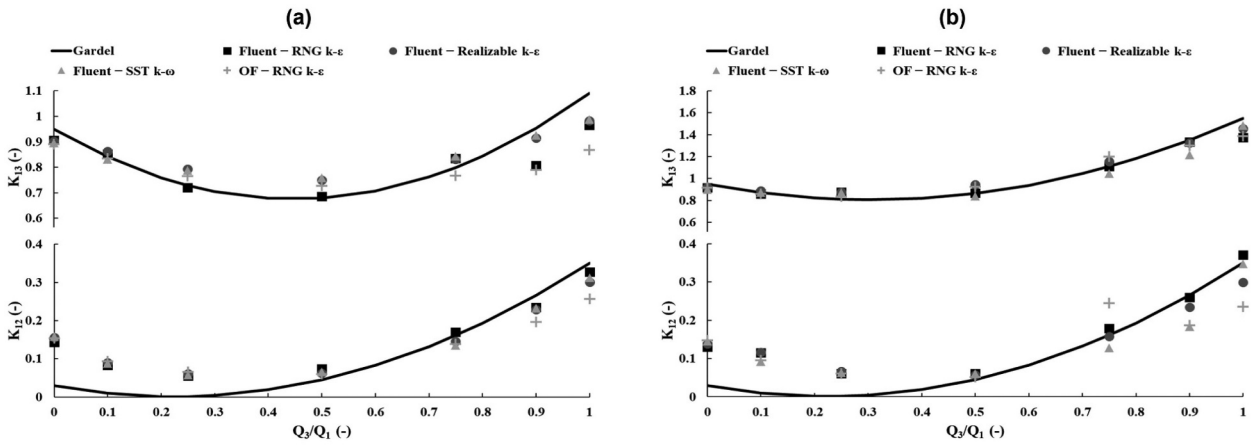

Figure 3. Comparison of the head loss coefficients K_{12} and K_{13} predicted by CFD with an analytical formula for (a) a T-junction at 100 degrees and (b) a T-junction at 80 degrees. The y-axis is deliberately clipped. OpenFoam (OF).

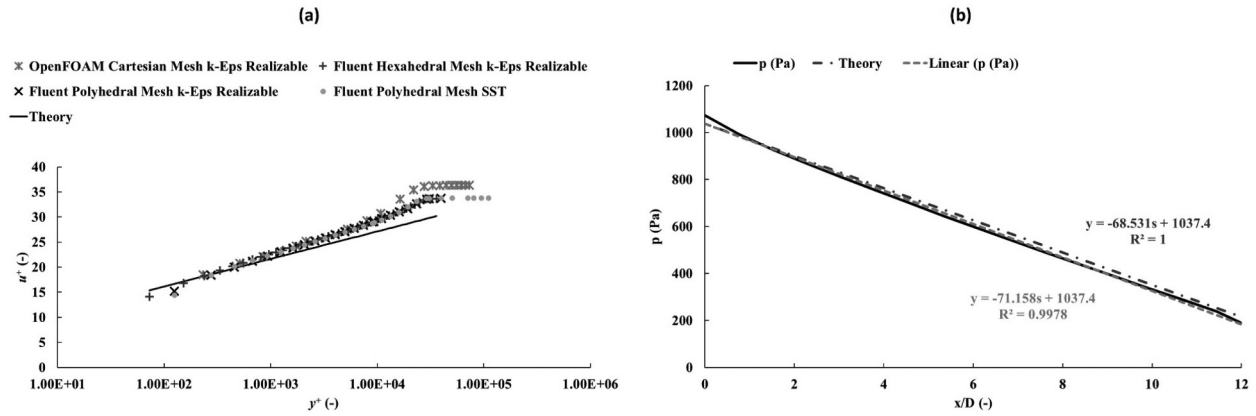

Figure 4. (a) Velocity profile in wall scale nine diameters downstream the inlet of pipe 1. (b) Streamwise pressure gradient along pipe 1 (OpenFOAM simulation with the realisable k-ε turbulence model). Y-junction at 80 degrees.

sometimes the case for some Fluent® simulations with the tetrahedral mesh.

3.2. Y-junction

A Y-junction is also considered for the validation of the CFD approach (Figure 1(b)). The diameter of pipes 1 and 3 is set to 2.25 m and the diameter of pipe 2 is set to 3 m, which are the diameters of the bifurcation CF2 considered in the next section. All three pipes have a length around 10 times the pipe diameter. The Reynolds number in pipe 1 is 9×10^6. For such a flow configuration, no analytical formula of the head loss coefficients has been found in the literature. Therefore, the development of the flow in pipe 1 has been compared with analytical formulae available for circular pipe flows to verify the accuracy of the simulation set-up. Figure 4(a) compares the dimensionless wall velocity u^+, defined as the velocity divided by the friction velocity (Bailly & Comte-Bellot, 2015), predicted by four different simulations and extracted nine diameters downstream of the inlet of pipe 1 with the theoretical logarithmic profile. Whatever the mesh (Cartesian, hexahedral or polyhedral) or turbulence model (SST or realisable k-ε), a logarithmic profile is followed by the simulations until y^+ values beyond 1000 and only small differences are observed between the simulations. However, due to the imposed uniform velocity profile at the inlet of pipe 1, the velocity profile is not fully developed and the corresponding von Kármán constant is lower than expected, with values around 0.32 instead of 0.41. The velocity profile at the wall is of primary importance in accurately computing the friction coefficient and, therefore, the streamwise pressure gradient. The pressure profile in the centre line of the pipe can be calculated analytically using Equations (11) and (12) (Mckeon et al., 2004).

$$p = -2\rho C_f C^2 \frac{x}{D} + B \tag{11}$$

$$\frac{1}{\sqrt{C_f}} = 3.86\log_{10}\left(\mathrm{Re_D}\sqrt{C_f}\right) - 0.088 \tag{12}$$

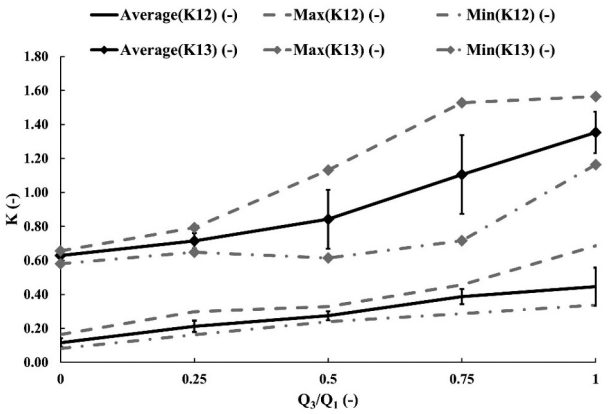

Figure 5. Statistical values of the head loss coefficients K_{12} and K_{13} predicted by CFD. The error bar denotes the standard deviation. Y-junction at 80 degrees.

Where C_f is the friction coefficient; C is the discharge velocity; x/D is the dimensionless pipe length; B is an arbitrary constant; and $\mathrm{Re_D}$ is the Reynolds number based on the pipe diameter. Figure 4(b) compares the simulated and analytical streamwise pressure profiles, for which the slopes differ by less than 4%.

In total, 79 simulations were performed to investigate the influence of the mesh, the turbulence model, the boundary conditions and the solver. Figure 5 shows the average, standard deviation, minimum and maximum values of the head loss coefficients K_{12} and K_{13} for a discharge ratio range between 0 and 1. Both head loss coefficients follow almost a linear relationship regarding the discharge ratio, which is different from the T-junction (see Table 2). For the head loss coefficient K_{12}, the dispersion between the simulations increases with the discharge ratio as for the T-junctions. The standard deviation reaches 25% of the average value for a discharge ratio of 1, i.e. when there is no flow in pipe 2, instead of 15% for a lower discharge ratio. Regarding the head loss coefficient K_{13}, the dispersion between the simulations is low for low discharge ratios (0 and 0.25) but increases for higher discharge ratios and reaches its maximum for

Table 2. Ranking of the bifurcations from the largest to the smallest value of the head loss coefficient K_{13} for a discharge ratio around 0.7, with the trend of the head loss coefficient K_{13} as a function of the discharge ratio. The quantity $\widehat{K_{13}}$ denotes the average value of the head loss coefficient K_{13} over all the discharge ratios computed. θ is the angle between pipes 1 and 3, whereas β is the angle between pipes 1 and 2.

Bifurcation	θ (°)	β (°)	K_{13} at $Q_3/Q_1 \approx 0.7$	$\widehat{K_{13}}$	Trend	R^2
Intra-group (FMHL)	77	103	1.36	1.47	Constant	
Inter-house V2 to V1 (FMHL)	34	34	1.28	1.09	Linear	0.99
T-junction	80	0	1.13	1.06	Quadratic	1.00
Y-junction	80	40	1.11	0.93	Linear	0.95
Inter-house V1 to V2 (FMHL)	34	0	1.05	0.91	Quadratic	0.88
Inter-group G5 to G6 (FMHL)	44	44	1.04	0.89	Linear	0.93
T-junction	90	0	0.94	0.93	Quadratic	1.00
CF2 (Grand'Maison)	80	22	0.91	0.81	Quadratic	0.96
T-junction	100	0	0.82	0.84	Quadratic	0.97
Inter-group G6 to G5 (FMHL)	44	0	0.49	0.56	Quadratic	0.93

a discharge ratio of 0.75. For this ratio, the CFD results range from 0.7 to 1.5 with an average value of 1.1.

Figure 6 compares the average value of the head loss coefficient K_{13} depending on the turbulence model or the mesh used. The mesh does not have a strong influence on the predicted average value, whereas it is noticeable that the RNG k-ε turbulence model predicts an average value larger than the one predicted by the SST or the realisable k-ε turbulence models. Consequently, the main explanation for the large dispersion of the results for a discharge ratio of 0.75 is due to the turbulence model.

Figures 7 and 8 display the streamlines and an iso-surface of the Q-criterion (value of $10s^{-2}$) coloured by the velocity for the discharge ratio of 0.75 predicted by the simulation performed with the Ansys® Fluent® software on the hexahedral mesh. The realisable k-ε

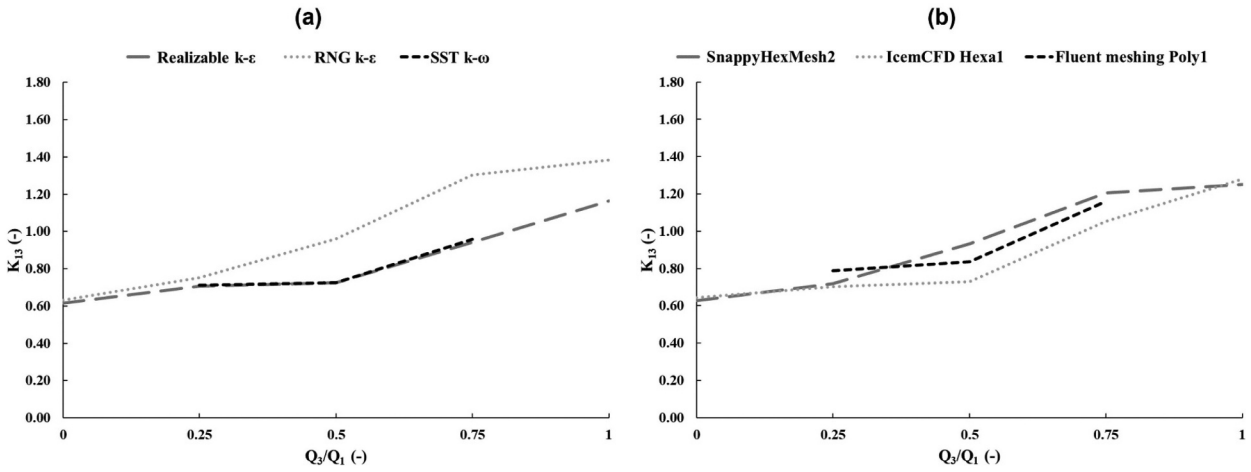

Figure 6. Average value of the head loss coefficient K_{13}: (a) for three different turbulence models, (b) for three different meshes.

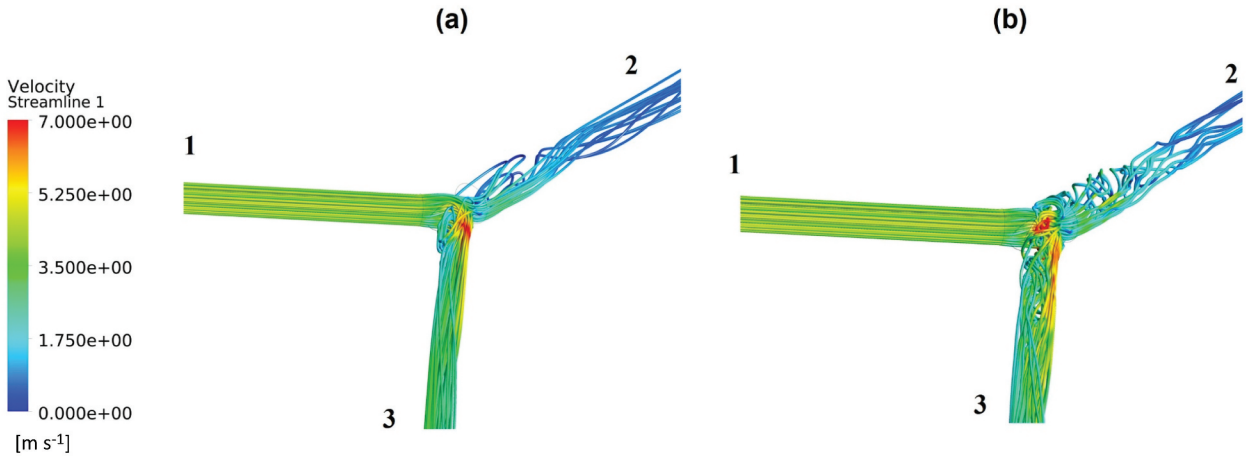

Figure 7. Streamlines coloured by the velocity magnitude. (a) Realisable k-ε turbulence model; (b) RNG k-ε turbulence model. Discharge ratio of 0.75. Simulations performed with the Ansys® Fluent® software with the mesh ICEM CFD™ Hexa1. Y-junction at 80 degrees.

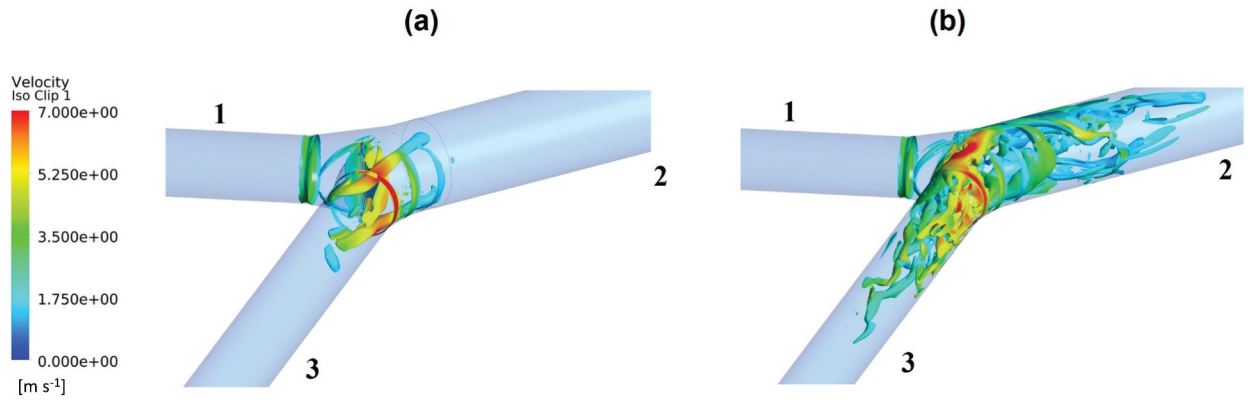

Figure 8. Iso-surface of the Q-criterion (value of $10s^{-2}$) coloured by the velocity magnitude. (a) Realisable k-ε turbulence model; (b) RNG k-ε turbulence model. Discharge ratio of 0.75. Simulations performed with the Ansys® Fluent® software with the mesh ICEM CFD™ Hexa1. Y-junction at 80 degrees.

turbulence model predicts a solution with a weak roll-up of the streamlines and small vortical structures compared to the RNG k-ε turbulence model. This kind of "unsteady" solution predicted by the latter model is the explanation for the highest head loss coefficients observed. This explanation is enforced by the fact that carrying out an unsteady-state simulation with the realisable k-ε turbulence model leads to an increase in the K_{13} value from 0.7 to 0.95, whereas the K_{13} value is still around 1.2 with the RNG k-ε turbulence model (the K_{12} keeps its steady value with both models). However, since this feature is not observed for the T-junction and no experimental data are available, it is not possible to determine which turbulence model provides better results.

4. Application to the investigation of HSC operating modes in two power plants

4.1. Description of the test cases

The main objective behind the simulations of the flow in junctions is to investigate the possibility to implement or to extend the HSC operating mode at the power plants of Grand'Maison (Decaix et al., 2021; Decaix, Drommi et al., 2022) and FMHL/FMHL+ (Decaix, Mettille et al., 2022).

The Grand'Maison power plant, located in the French Alps and owned by Electricité de France (EDF), is the largest pump-storage power plant in Europe, featuring four Pelton turbines in a powerhouse at ground level and eight pump-turbines in an underground powerhouse (Figure 9(a)), for a maximum capacity of 1240 MW in pump mode and 1800 MW in turbine mode. The HSC mode can be implemented following two different routes: the short route, i.e. the pumped flow is diverted to the Pelton turbine(s) that is/are fed by the same penstock (CF1, CF2 or CF3 in Figure 9(a)); or the long route, i.e. the pumped flow is diverted to the Pelton turbine(s) that is/are fed by another penstock. Only the short route is considered in this paper. For the long route, the reader is referred to a previous publication (Decaix, Drommi et al., 2022).

The FMHL/FMHL+ power plant is characterised by two powerhouses (Figure 9(b)): Veytaux 1, featuring

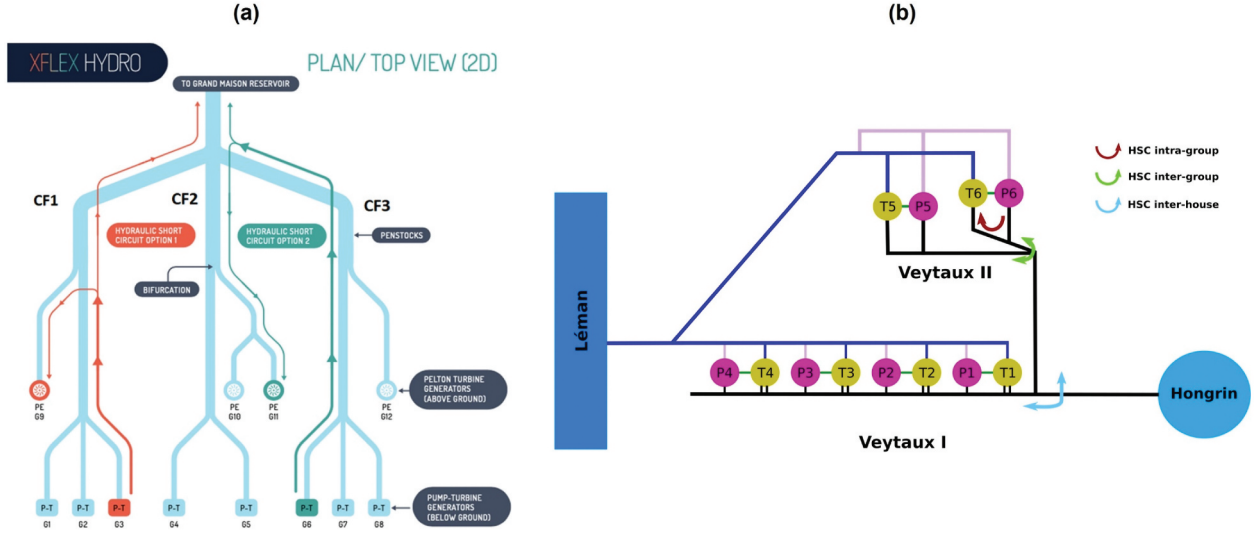

Figure 9. (a) Layout of the Grand'Maison power plant with the two different routes for the HSC mode. (b) Layout of the FMHL/FMHL+ power plant with the three different possible HSC modes: intra-group, inter-group and inter-house.

four horizontal ternary groups of 60 MW each consisting of two two-jet Pelton turbines and a five-stage centrifugal pump, in operation since 1971; Veytaux 2, featuring two vertical ternary groups (groups 5 and 6) of 120 MW each consisting of a five-jet Pelton turbine and a five-stage centrifugal pump, in operation since 2016. The HSC mode is already in operation at Veytaux 2 between the pump and the turbine of a same group (group 5 or 6), and it is referred to as intra-group HSC mode in this paper. Two other HSC configurations are possible but not permitted: the inter-group HSC mode between the pump of group 5 (group 6) and the turbine of group 6 (group 5); and the inter-house HSC mode between the two powerhouses of Veytaux 1 and Veytaux 2.

Overall, five bifurcations (Figure 10) are considered for the CFD investigation: two for the Grand'Maison power plant (due to the symmetry of penstocks 1 and 3) and three for the FMHL/FMHL+ power plant. The two bifurcations of Grand'Maison are rather of the Y-junction type but with pipes 1 and 2 aligned for the bifurcation CF1 and slightly misaligned for the bifurcation CF2 (the green part in Figure 10(b) is the same geometry as the green part in Figure 1(b)). In HSC mode, the bifurcation in the penstock CF1 links three pump-turbines with one Pelton turbine, whereas the bifurcation in the penstock CF2 links two pump-turbines with two Pelton turbines.

The FMHL/FMHL+ power plant features three bifurcations: the intra-group bifurcation (Figure 10 (c)) is a T-junction at 77 degrees; the inter-group and inter-house bifurcations are rather of Y-junction type with the particularity that the flow in pipes 1 and 3 can be in either direction depending on which group or powerhouse is in pumping mode (in Figure 10(d,e), the pipe numbering is adjusted to always have an inflow in pipe 1 and an outflow in pipe 3). For this test case, the reader can refer to a recent paper for more details, mainly regarding the influence of the curvature correction term (Decaix, Mettille et al., 2022).

For the whole set of simulations, the Reynolds number ranges from 2×10^6 to 30×10^6 and the number of simulations per junction ranges from 40 to 64.

4.2. Head loss coefficients

Figure 11 provides the average and standard deviation of the head loss coefficients K_{12} and K_{13} for a discharge ratio range between 0 and 1 and for each bifurcation considered in the present paper. For the inter-group and inter-house HSC modes at the FMHL/FMHL+ power plant, the distinction is made depending on the flow direction going from group 5 (group 6) to group 6 (group 5) or from Veytaux 1 (Veytaux 2) to Veytaux 2 (Veytaux 1).

Regarding the head loss coefficient K_{12} (i.e. between the pump and the reservoir), the maximum average values, at least twice larger than for the other configurations, are obtained for the intra-group bifurcation. This result is expected since this is the configuration with the largest angle β between pipes 1 and 2 (see Table 2). Furthermore, it is the configuration for which the standard deviation is the highest, around 25% of the average value. It is also interesting to notice that the average values for the inter-group and inter-

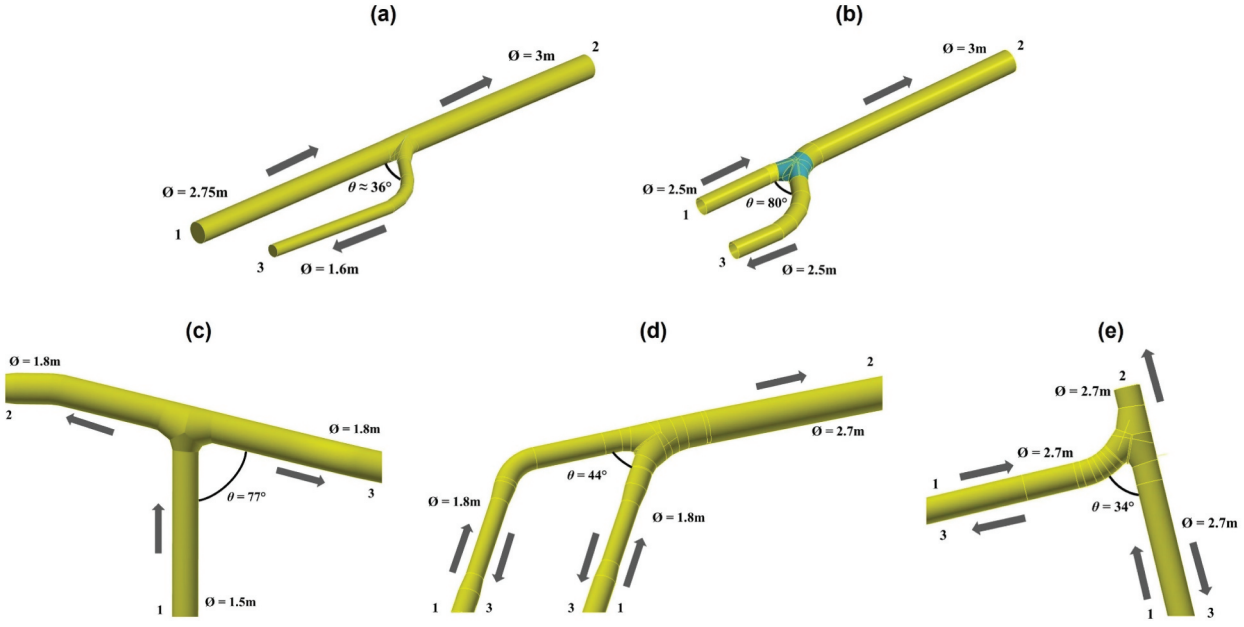

Figure 10. (a, b) Geometries of the bifurcations at the Grand'Maison power plant on the penstocks CF1 and CF2, respectively. (c–e) Geometries of the intra-group, inter-group and inter-house bifurcations, respectively, at the FMHL/FMHL+ power plant. The arrows indicate the flow direction in each pipe. Pipe 1 is always the pipe linked to the pump(s), pipe 2 the one linked to the upper reservoir and 3 the one linked to the turbine(s). For (d) and (e), the pipe numbering is adapted depending on the flow direction.

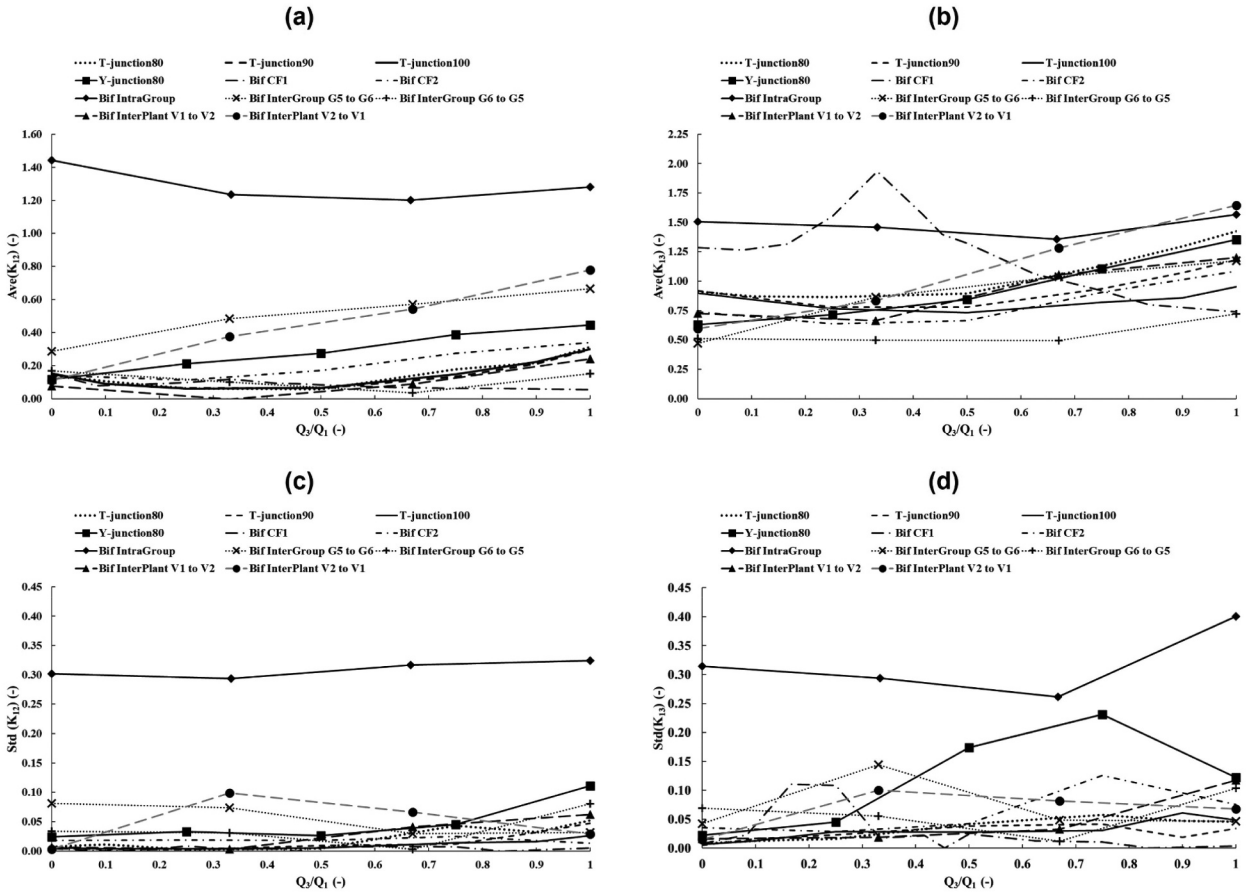

Figure 11. (a, b) average value and (c, d) standard deviation of the head loss coefficients K_{12} and K_{13}, respectively. Each line corresponds to one geometry and one flow direction. G5 and G6 refer to groups 5 and 6 of the FMHL/FMHL+ power plant. V1 and V2 refer to the powerhouses Veytaux 1 and Veytaux 2 of the FMHL/FMHL+ power plant.

house bifurcations have significant differences depending on the flow direction. For the inter-group bifurcation, the value of the coefficient K_{12} is multiplied by 4 for the flow direction from group 5 to group 6 compared to the opposite direction, which is also in relation with the value of the angle β. The larger the angle β, the larger the head loss coefficient K_{12}.

Regarding the head loss coefficient K_{13} (i.e. between the pump(s) and the turbine(s)), the shape of the curve for the bifurcation CF1 needs to be clarified. For this bifurcation, the HSC mode can be operated with three pump-turbines in pump mode and one Pelton turbine (Figure 9(a)). By consequence, the maximum pumped discharge corresponds to a discharge ratio around 0.35, for which the head loss coefficient K_{13} reaches its maximum value close to 2. Furthermore, this is the only bifurcation with a contraction of the pipe diameters, with a diameter of pipe 3 equal to 60% of the diameter of pipe 1, which increases the head losses. Apart from this configuration, the values range from 0.5 to 1.5, which means that the geometrical shape of the bifurcation has a non-negligible influence on the head loss coefficients. As for the K_{12} coefficient, the maximum average values are once again observed for the intra-group bifurcation, followed closely for discharge ratios above 0.6 by the inter-house bifurcation with the flow from Veytaux 2 to Veytaux 1. The direction of the flow in the bifurcation also influences the head loss coefficient, with, for instance, a value that can double for the inter-group bifurcation depending on the flow direction. The standard deviation is also maximum for the intra-group bifurcation with values around 20% of the average values that is at least twice higher than those for the other configurations, except the Y-junction at 80 degrees and discharge ratios between 0.5 and 0.8.

Table 2 ranks the different bifurcations, except bifurcation CF1, from the largest to the smallest value of the head loss coefficient K_{13} for a discharge ratio around 0.7. This ranking is close to the one that would be based on the average value $\widehat{K_{13}}$ computed over all the discharge ratios (shown also in Table 2). In addition, Table 2 provides the values of the angles θ and β and the trend of the relationship between K_{13} and the discharge ratio, with the value of the coefficient of determination (R^2). It is noticeable that the highest values of K_{13} are related to a constant or a linear trend rather than a quadratic relationship. For the inter-group and inter-house bifurcations, the change in the flow direction is linked to a change in the angle β: the

higher the angle β, the higher the coefficient K_{13}. This is also verified by comparing the Y-junction and the bifurcation CF2, which have the same geometry for the bifurcation but with a slightly different angle β. The influence of the angle θ is less evident. For the T-junctions: the higher the θ angle, the lower the K_{13} coefficient. This is also the case when comparing the inter-group and the inter-house bifurcations for an angle β = 0. However, the inter-group bifurcation with an angle θ of 44 degrees has a lower K_{13} value than the T-junction at 100 degrees even if in both cases the angle β is null.

4.3. Flow topology

The flow topology is investigated by focusing on the streamlines and the iso-surface of the Q-criterion coloured by the magnitude of the velocity field.

Figures 12 and 13 compare the flow topology between the bifurcations CF1 and CF2 of the Grand'Maison power plant for a discharge ratio of 0.75 computed using either the realisable k-ε or the RNG k-ε turbulence model. For both bifurcations, the RNG k-ε turbulence model predicts a more "unstable" flow than the realisable k-ε turbulence model, as observed for the Y-junction at 80 degrees. This point is particularly emphasised by the iso-surface of the Q-criterion that shows the development of several small vortices in pipe 3 downstream of the bifurcation for the RNG k-ε turbulence model. The number of vortices is smaller for the bifurcation CF1 than for CF2 due to the lower diameter of pipe 3 compared to pipe 1 for this geometry. Consequently, the flow converges and the re-circulation zone just downstream of the bifurcation is smaller, as is clearly visible when comparing the streamlines obtained with the realisable k-ε turbulence model (Figure 12(a, b)). This point also explained the larger standard deviation observed for the bifurcation CF2 regarding the head loss coefficient K_{13} (Figure 11 (b)). Another interesting feature is the quick damping of the vortical structures since only a few vortices are still present in the outlet section of pipe 3, which means that the flow realigned more quickly with the pipe direction than in turbine mode (see Figure 5 in Decaix et al., 2021).

Figure 14 displays the streamlines and the iso-surface of the Q-criterion in the intra-group bifurcation of the FMHL/FMHL+ power plant for a discharge ratio of 0.66. Due to the large values of both angles θ and β, the flow splits at the junction and rolls up in pipes 2 and 3, leading to the development of a swirling flow that could deteriorate the quality of the flow at the inlet of the turbines. This feature is the reason that

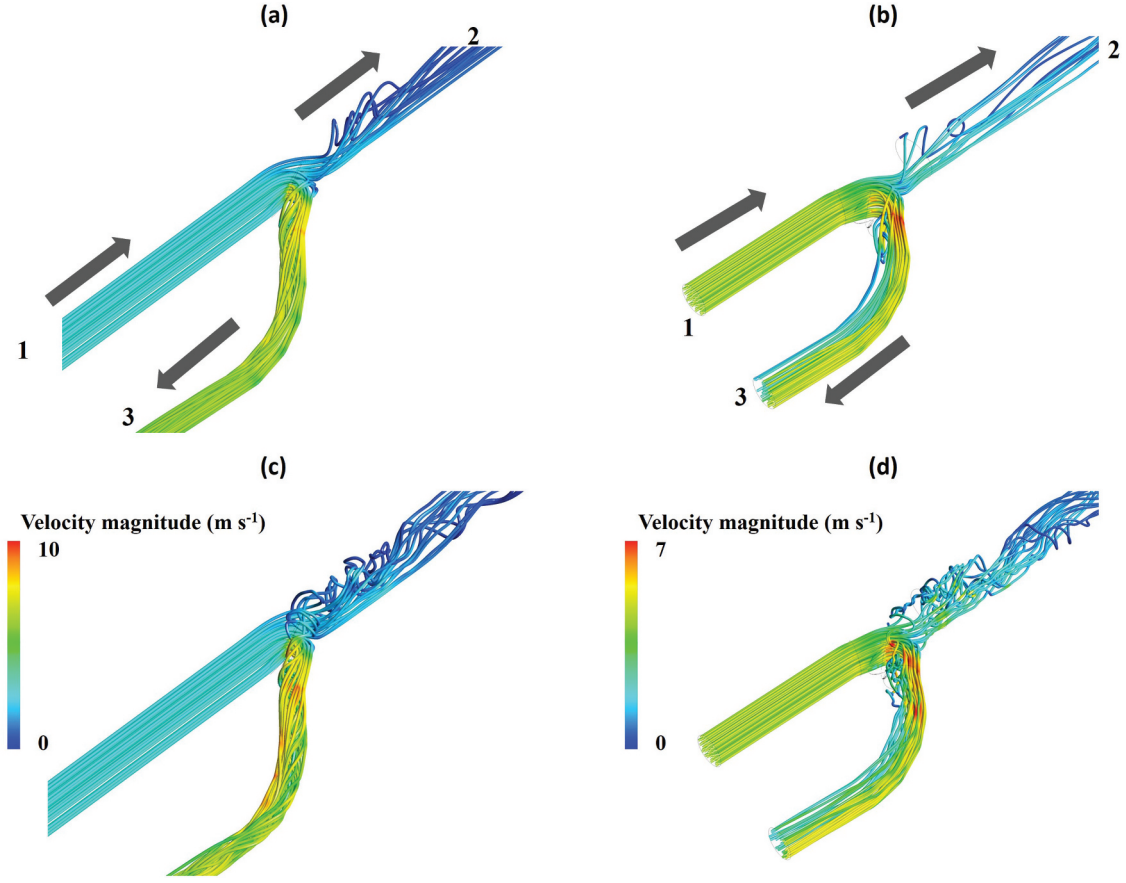

Figure 12. Streamlines coloured by the velocity magnitude (the scale is the same for (a) and (c) and for (b) and (d)). (a, c) Bifurcation CF1; (b, d) bifurcation CF2. (a, b) Simulations with the realisable k-ε turbulence model; (c, d) simulations with the RNG k-ε turbulence model. Discharge ratio of 0.75. The arrows indicate the flow direction.

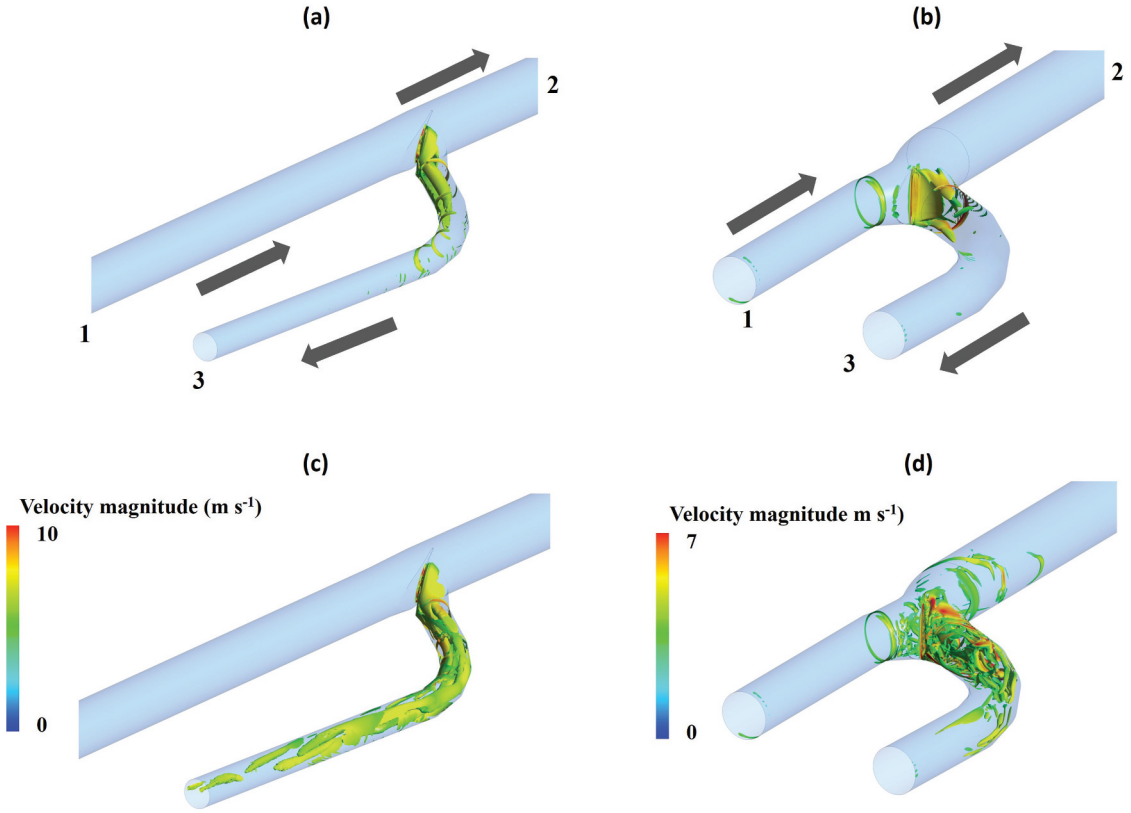

Figure 13. Iso-surface of the Q-criterion, value of $10s^{-2}$, coloured by the velocity magnitude (the scale is the same for (a) and (c) and for (b) and (d)). (a, c) Bifurcation CF1; (b, d) bifurcation CF2. (a, b) Simulations with the realisable *k-ε* turbulence model; (c, d) simulations with the RNG *k-ε* turbulence model. Discharge ratio of 0.75. The arrows indicate the flow direction.

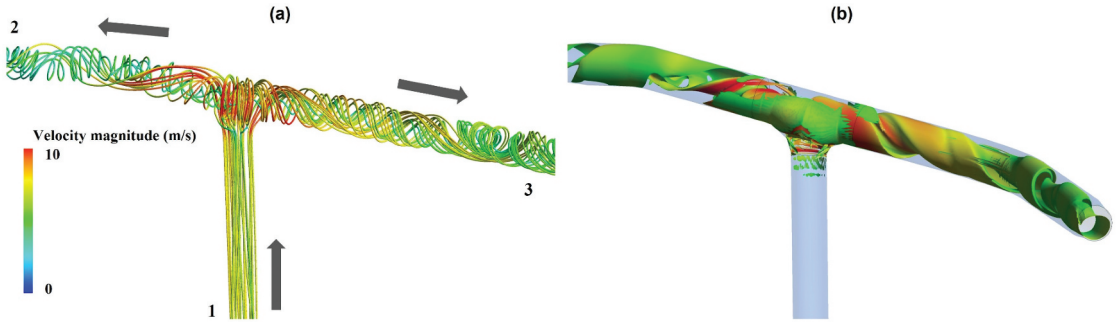

Figure 14. (a) Streamlines and (b) iso-surface of the Q-criterion (value of $20s^{-2}$) coloured by the velocity magnitude. Intra-group bifurcation of the FMHL/FMHL+ power plant. Simulations with the SST turbulence model. Discharge ratio of 0.66. The arrows indicate the flow direction.

prevents the operation of the machines in HSC mode beyond a discharge ratio of 0.66.

Figures 15 and 16 compare the streamlines and the iso-surface of the Q-criterion in the inter-group and inter-house bifurcations of the FMHL/FMHL+ power plant according to the flow direction in the bifurcation. As noticed in the previous sub-section, the value of the head loss coefficient K_{13} depends on the flow direction in the bifurcation (Figure 11(b)). By looking at the iso-surface of the Q-criterion, it appears that the development of long streamwise vortices in pipe 3 (Figures 15(d) and 16(c)) is correlated with a lower head loss coefficient. This seems counterintuitive. However, the streamlines show that high values of the coefficient K_{13} are related to a stronger "impingement" of the flow on the opposite wall to pipe 1 due to an angle β larger than 0. Consequently, for the HSC configurations between the groups 5 and 6 (Figure 15(a)) and the houses Veytaux 2 and Veytaux 1 (Figure 16(b)), the flow from pipe 1 impinges on the opposite wall, inducing rapid changes in both the fluid velocity and the fluid direction. These two phenomena are less pronounced, or even absent, when the flow is in the opposite direction (Figures 15(b) and 16(a)) due to the alignment of pipes 1 and 2 ($\beta = 0$). It appears that the smaller the "impinging" flow, the lower the coefficient K_{13}.

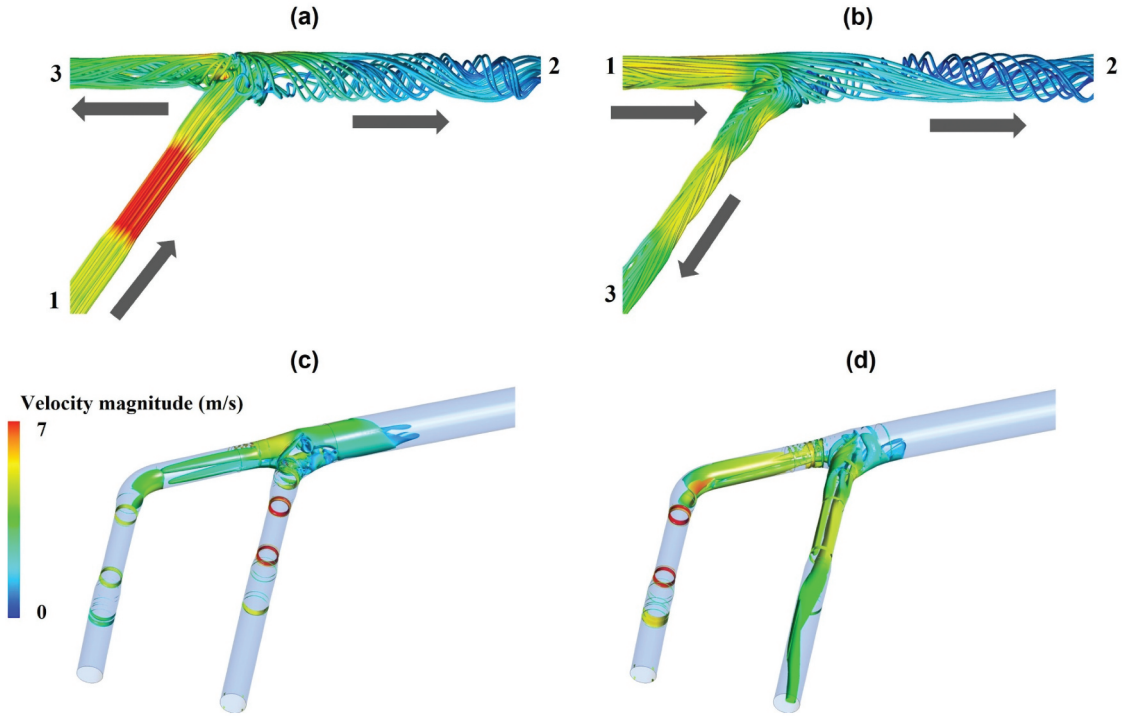

Figure 15. (a, b) Streamlines and (c, d) iso-surface of the Q-criterion, value of 2 s^{-2}, coloured by the velocity magnitude. Inter-group bifurcation of the FMHL/FMHL+ power plant. (a, c) HSC mode between groups 5 and 6; (b, d) HSC mode between groups 6 and 5. Simulations with the SST turbulence model. Discharge ratio of 0.66.

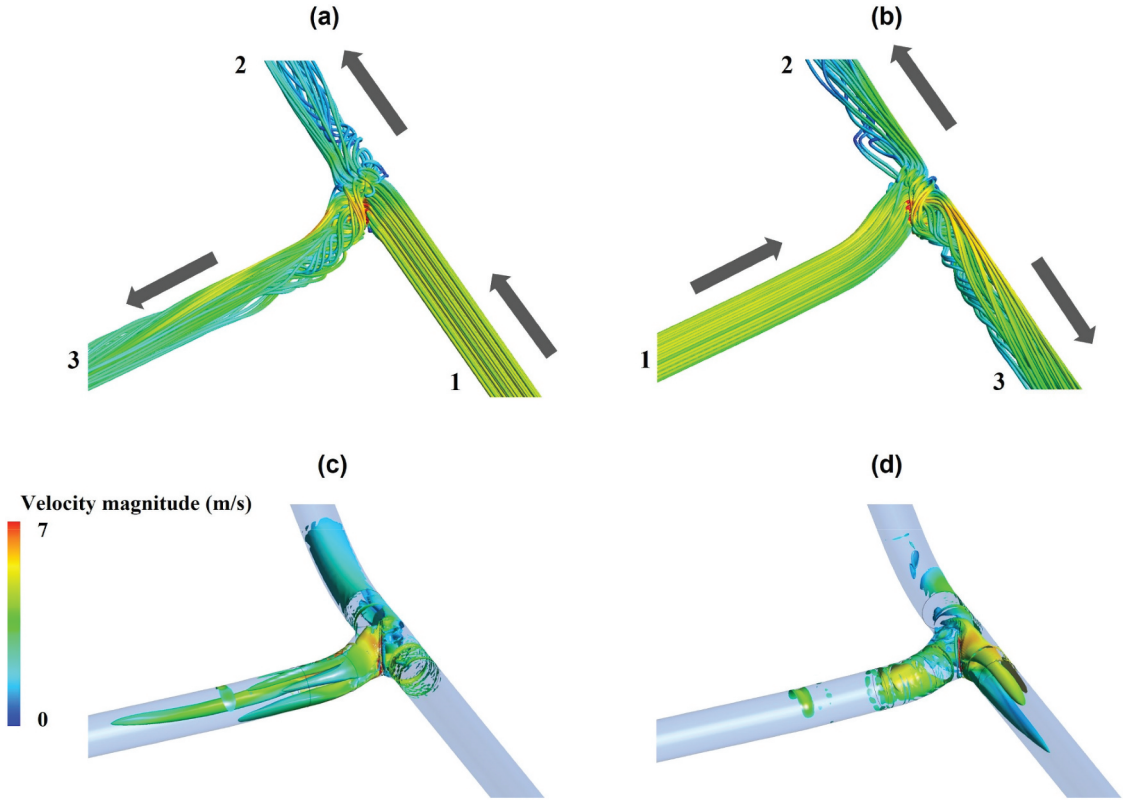

Figure 16. (a, b) Streamlines and (c, d) iso-surface of the Q-criterion (value of 1 s^{-2}) coloured by the velocity magnitude. Inter-house bifurcation of the FMHL/FMHL+ power plant. (a, c) HSC mode between Veytaux 1 and Veytaux 2; (b, d) HSC mode between Veytaux 2 and Veytaux 1. Simulations with the SST turbulence model. Discharge ratio of 0.66.

4.4. Wall quantities

The wall shear stress and the wall pressure are also interesting quantities to verify whether the pipe walls undergo stress changes or if a risk of cavitation can occur.

Figure 17 compares the wall shear stress for the bifurcation CF2 between the turbine mode and the HSC mode for a discharge ratio of 0.75. The simulations are carried out with the realisable k-ε turbulence model in steady mode. It is obvious that the wall shear stress increases in HSC mode by a factor of around 6, with a maximum value located on the splitter between the two pipes. In the case of sediments transported, attention should be paid to avoid an accelerated abrasion of the coating.

Figure 18 shows, for the bifurcation CF2, the time-average and root Mean square error (RMSE) of the wall pressure computed with the RNG k-ε turbulence model in unsteady mode; 80s are simulated and the statistics are computed over the latest 20s, which represents 5 times the time it takes for a flow particle to flow from the inlet of pipe 1 to the outlet of pipe 3. The pressure fluctuations are highest in the recirculation area just downstream the bifurcation. The maximum value of the RMSE is around 30,000 Pa. By assuming a Gaussian distribution for the wall pressure, the maximum pressure fluctuations would be around 90,000 Pa, i.e. less than 2% of the gross head and 5 times lower than the static pressure variation due to the change in the water level in the upper reservoir. Therefore, no risk to the structure is expected. This point is also confirmed by the numerical work of Khalafaoui et al. (2022), who shows that the average and oscillating stress levels in HSC mode are comparable with the ones in turbine mode and well below the fatigue limit.

5. Conclusion

A CFD investigation of the flow in nine bifurcations was carried out with the objectives of validating the numerical set-up and improving knowledge of the flow in HSC mode, mainly regarding the head losses, the flow topology, the wall pressure and the wall shear stress.

First, the formula used to define the losses in a bifurcation is derived to avoid misunderstandings regarding the interpretation of the head loss coefficient K_{ij} considered in this paper. Following the present development, the coefficient K_{ij} is useful to compare different geometries at a given discharge ratio.

Regarding the validation of the numerical set-up, simulations of three T-junctions, for which analytical formulae of the head loss coefficients derived from experimental studies are available in literature, have been computed. The results show that the head loss coefficients are in good agreement with the analytical formulae, even if for the coefficient K_{12} it is necessary to

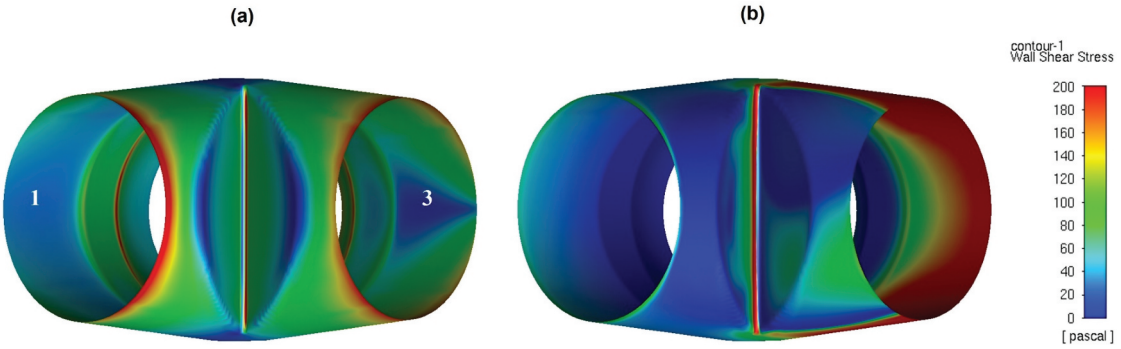

Figure 17. Wall shear stress on the wall of bifurcation CF2: (a) turbine mode and (b) HSC mode at a discharge ratio of 0.75. Simulations with the realisable k-ε turbulence model. The pipe numbering, 1 and 3, is added on the picture.

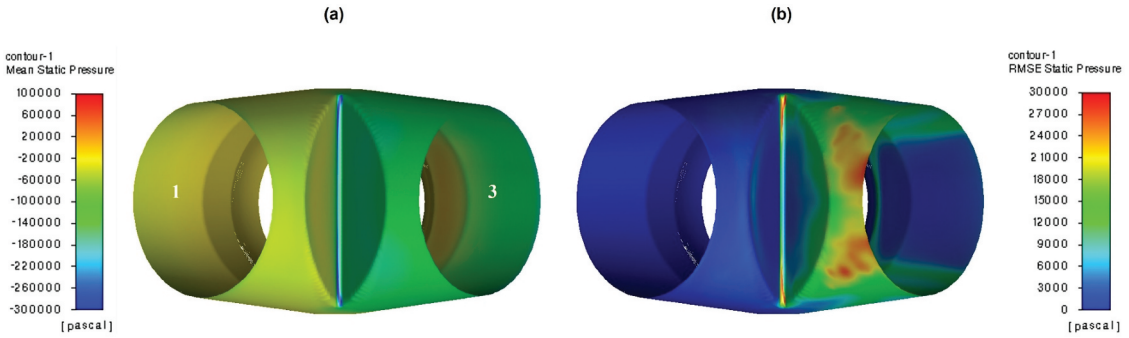

Figure 18. (a) Time-average pressure. (b) RMSE (Root Mean Squared Error) of the pressure on the wall of bifurcation CF2. Simulations with the RNG k-ε turbulence model. The pipe numbering, 1 and 3, is added on the picture.

set a developed velocity profile at the inlet of pipe 1. For the Reynolds number considered (above 5×10^6), a y^+ value around 200 is sufficient regardless of what mesh elements are considered (tetrahedral, polyhedral, hexahedral), and the turbulence model has almost no influence on the prediction of the head loss coefficients. A Y-junction has also been investigated despite the lack of experimental data. As for the T-junction, the mesh has no influence regarding the prediction of the head loss coefficients if the standard requirements are followed. However, an influence of the turbulence model is noticed for a discharge ratio around 0.75 since the realisable k-ε and the SST turbulence models predict a head loss coefficient K_{13} lower than the RNG k-ε turbulence model. No clear explanation for this has been found. However, the latest model predicts a more "unsteady" flow characterised by the presence of small vortices downstream of the bifurcation, which seems to be responsible for the higher losses. Carrying out unsteady-state simulations reduce the discrepancies between the turbulence models.

Application to five existing bifurcations of the Grand'Maison and FMHL/FMHL+ power plants was investigated using different software programs, meshes and turbulence models. The comparison of the head loss coefficients and the analysis of the flow topology show that the highest values of the head loss coefficients are related to the higher "impingement" of the flow to the opposite wall, which is driven by a combination of the values of the angles θ and β. For a given angle θ, the higher the β, the higher the K_{13}. A low value of the angle θ is a good choice for the turbine mode but can limit the operating range in HSC mode, and vice versa. However, a small angle θ coupled with a geometry that mimics the shape of a bend between pipes 1 and 3 with no sharp edges and sudden changes in the flow direction – such as the CF2 bifurcation – seems to be a good choice to limit the losses and the development of a swirling flow in HSC mode. Consequently, T-junctions are not recommended for new power plants designed to operate in HSC mode and can limit the operating range of existing power plants (as is the case at FMHL/FMHL+). In contrast, Y-junctions with an angle θ below 80 degrees, an angle β below 50 degrees and no pipe diameter changes should be a good compromise to provide good performance in pump, turbine and HSC modes.

The wall pressure fluctuations and the wall shear stresses increase in HSC mode compared to pump and turbine modes. Special attention should be paid to these two quantities, mainly in the case of low-head power plants and sediment transport due to the risk of cavitation and accelerated erosion.

Steady-state Reynolds-Averaged Navier-Stokes (RANS) simulations seem to be sufficient to investigate the flow in HSC mode for most of the interesting quantities (head loss coefficients, flow topology, wall quantities) with an accuracy of around 15% for the head losses, for instance, in the range of the discrepancy between the empirical formulae. Unsteady-state RANS simulations are required only in the case of large discrepancies between the different turbulence models or if wall pressure fluctuations are needed for specific investigations.

These new results for the hydropower community can be used as guidelines to investigate whether existing power plants are suitable for implementing HSC operating modes and can be used in designing new power plants with junctions suitable for being operated in HSC mode.

Nomenclature

C	Discharge velocity in m s^{-1}
C_f	Friction coefficient
D	Pipe diameter in m
g	Gravitational acceleration in m s^{-2}
k	Turbulent kinetic energy in m^2 s^{-2}
$K_{i,j}$	Head loss coefficient
p	Pressure in Pa
$\overline{p_{tot}}$	Surface average total pressure in Pa
P	Power in W
Q_v	Volumetric flow rate in m^3 s^{-1}
Re_D	Reynolds number based on the pipe diameter
S	Surface section in m^2
u^+	Dimensionless wall velocity
y^+	Dimensionless wall distance
z	Piezometric head in m
$\boldsymbol{c}$	Velocity vector
$\boldsymbol{n}$	Surface normal unit vector
β	Angle between pipe 1 and pipe 2
ε	Turbulent energy dissipation rate in m^2 s^{-3}
γ	Discharge ratio
ρ	Fluid density in kg m^{-3}
θ	Angle between pipe 1 and pipe 3
CFD	Computational fluid dynamics
HSC	Hydraulic short circuit
RANS	Reynolds-averaged Navier-Stokes
RNG	Renormalisation group
SST	Shear-stress transport

Disclosure statement

No potential conflict of interest was reported by the author(s).

Funding

The present study was supported by the European Union's Horizon 2020 research and innovation programme [grant agreement No. 857832] and the Bundesamt für Energie [grant SI/502106].

ORCID

Jean Decaix http://orcid.org/0000-0003-3944-471X
Cécile Münch-Alligné http://orcid.org/0000-0003-3362-6248

Data availability statement

The data can be made available depending on the application targeted. Please contact the corresponding author for further information.

References

Bailly, C., & Comte-Bellot, G. (2015). *Turbulence*. Springer-Verlag GmbH.

Comolet, R. (2006). *Mécanique expérimentale des fluides – Tome 2 – 4ème édition*. Dunod.

Decaix, J., Biner, D., Drommi, J.-L., Avellan, F., & Münch-Alligné, C. (2021). CFD simulations of a Y-junction for the implementation of hydraulic short-circuit operating mode. *IOP Conference Series: Earth and Environmental Science*, *774*(1), 012013. https://doi.org/10.1088/1755-1315/774/1/012013

Decaix, J., Drommi, J.-L., Avellan, F., & Münch-Alligné, C. (2022). CFD simulations of hydraulic short-circuits in junctions, application to the Grand'Maison power plant. *IOP Conference Series: Earth and Environmental Science*, *1079*(1), 012106. https://doi.org/10.1088/1755-1315/1079/1/012106

Decaix, J., Mettille, M., Hugo, N., Valluy, B., & Münch-Alligné, C. (2022). CFD investigation of the hydraulic short-circuit mode in the FMHL+ pumped storage power plant. *ViennaHydro conference 2022*, Vienna, Austria.

Durbin, P. (2011). *Statistical theory and modeling for turbulent flows*. Wiley.

France's Grand Maison plant testing HSC technology. (2022). *International water power & dam construction*. https://www.waterpowermagazine.com/news/newsfrances-grand-maison-plant-testing-hsc-technology-9767457

Gardel, A. (1957a). Les pertes de charge dans les écoulements au travers de branchements en té. *Bulletin Technique de La Suisse Romande*, *10*, 143–148. https://www.e-periodica.ch/cntmng?pid=bts-002:1957:83::71

Gardel, A. (1957b). Les pertes de charges dans les écoulements au travers de branchements en té. *Bulletin Technique de La Suisse Romande*, *9*, 123–130. https://www.e-periodica.ch/cntmng?pid=bts-002:1957:83::76

Guittet, M., Capezzali, M., Gaudard, L., Romerio, F., Vuille, F., & Avellan, F. (2016). Study of the drivers and asset management of pumped-storage power plants historical and geographical perspective. *Energy*, *111*, 560–579. https://doi.org/10.1016/j.energy.2016.04.052

Huber, B., Korger, H., & Fuchs, K. (2005). Hydraulic optimization of a T-junction - hydraulic model tests and CFD-simulation. *XXXI IAHR Congress*, Seoul, Korea.

Karpenko, M., Stosiak, M., Šukevičius, Š., Skačkauskas, P., Urbanowicz, K., & Deptuła, A. (2023). Hydrodynamic processes in angular fitting connections of a transport machine's hydraulic drive. *Machines*, *11*(3), 355. https://doi.org/10.3390/machines11030355

Khalfaoui, K., Tismer, A., & Riedelbauch, S. (2022). Numerical investigation of the structural behaviour of a headwater bifurcation in hydraulic short circuit. *IOP Conference Series: Earth and Environmental Science*, *1079*(1), 012078. https://doi.org/10.1088/1755-1315/1079/1/012078

Landry, C., Nicolet, C., Badina, C., Pichon, H., & Drommi, J.-L. (2022). Contribution for the roadmap of hydraulic short circuit implementation: Case of Grand-Maison pumped storage power plant. *IOP Conference Series: Earth and Environmental Science*, *1079*(1), 012107. https://doi.org/10.1088/1755-1315/1079/1/012107

Martinot, E. (2016). Grid integration of renewable energy: Flexibility, innovation, and experience. *Annual Review of Environment and Resources*, *41*(1), 223–251. https://doi.org/10.1146/annurev-environ-110615-085725

Mckeon, B. J., Swanson, C. J., Zagarola, M. V., Donnelly, R. J., & Smits, A. J. (2004). Friction factors for smooth pipe flow. *Journal of Fluid Mechanics*, *511*, 41–44. https://doi.org/10.1017/S0022112004009796

Menter, F. R. (2009). Review of the shear-stress transport turbulence model experience from an industrial perspective. *International Journal of Computational Fluid Dynamics*, *23*(4), 305–316. https://doi.org/10.1080/10618560902773387

Menter, F. R., Lechner, R., & Matyushenko, A. (2021). *Best practice: RANS turbulence modeling in ansys CFD* (Technical Report 1.0). https://www.ansys.com/content/dam/amp/2022/march/quick-request/Best%20Practice%20RANS%20Turbulence%20Modeling%20in%20Ansys%20CFD.pdf

Meusburger, P. (2009). KOPS II on the grid – First experiences and lessons learned. *Hydro2009*.

Micoulet, G., Jaccard, A., & Rouge, N. (2016). FMHL+: Power extension of the existing Hongrin-Léman powerplant: From the first idea to the first kWh. *Hydro 2016*, Montreux, Switzerland.

Morabito, A., Wu, C., Sigali, S., & Vagnoni, E. (2022, November). CFD simulation for hydraulic short circuit feasability analysis. *ViennaHydro 2022*, Vienna, Austria.

Nicolet, C., Béguin, A., Dayer, J.-D., & Micoulet, G. (2019). Hydraulic transient challenges for the upgrade of FMHL+ pumped storage power plant from 240MW to 420MW. *IOP Conference Series: Earth and Environmental Science*, *240*, 052026. https://doi.org/10.1088/1755-1315/240/5/052026

Pérez-Díaz, J. I., Cavazzini, G., Blázquez, F., Platero, C., Fraile-Ardanuy, J., Sánchez, J. A., & Chazarra, M. (2014). *Technological developments for pumped-hydro energy storage* [Techreport]. Mechanical Storage Subprogramme, Joint Programme on Energy Storage, European Energy Research Alliance.

Pérez-Díaz, J. I., Sarasúa, J. I., & Wilhelmi, J. R. (2014). Contribution of a hydraulic short-circuit pumped-storage power plant to the load–frequency regulation of an isolated power system. *International Journal of Electrical Power & Energy Systems*, *62*, 199–211. https://doi.org/10.1016/j.ijepes.2014.04.042

Rennels, H. (2012). *Pipe flow*. John Wiley & Sons. https://www.ebook.de/de/product/18352127/rennels_hudson_pipe_flow.html

Shih, T.-S., Liou, W. W., Shabbir, A., Yang, Z., & Zhu, J. (1994). *A new k-e eddy viscosity model for high Reynolds number turbulent flows-model development and validation* (NASA Technical Memorundum 106721).

Wallin, S., & Johansson, A. V. (2000). An explicit algebraic Reynolds stress model for incompressible and compressible turbulent flows. *Journal of Fluid Mechanics*, *403*, 89–132. https://doi.org/10.1017/S0022112099007004

Ward-Smith, A. J. (1980). *Internal fluid flow: The fluid dynamics of flow in pipes and ducts*. Clarendon Press Oxford University Press.

Yakhot, V., Orszag, S. A., Thangam, S., Gatski, T. B., & Speziale, C. G. (1992). Development of turbulence models for shear flows by a double expansion technique. *Physics of Fluids A: Fluid Dynamics*, *4*(7), 1510–1520. https://doi.org/10.1063/1.858424